INSTITUTE OF PHYSICS PUBLISHING PLASMA PHYSICS AND CONTROLLED FUSION

Plasma Phys. Control. Fusion **47** (2005) 269–280 doi:10.1088/0741-3335/47/2/005

Spatially resolved characterization of electrostatic fluctuations in the scrape-off layer of the CASTOR tokamak

P Devynck[1], G Bonhomme[2], E Martines[3], J Stöckel[4], G Van Oost[5], I Voitsekhovitch[6], J Adámek[4], A Azeroual[6], F Doveil[6], I Ďuran[4], E Gravier[2], J Gunn[1] and M Hron[4]

[1] Association EURATOM-CEA, CEA/DSM/DRFC centre de Cadarache, 13108 Saint Paul Lez Durance, France
[2] Université Henri Poincaré, Vandoeuvre les Nancy, France
[3] Consorzio RFX, Associazione EURATOM-ENEA sulla Fusione, Padova, Italy
[4] Institute of Plasma Physics, Association EURATOM-IPP.CR, Prague, Czech Republic
[5] Department of Applied Physics, Ghent University, Belgium
[6] Equipe Turbulence Plasma, Laboratoire PIIM, Université de Provence, Marseille, France

Received 24 May 2004, in final form 10 September 2004
Published 11 January 2005
Online at stacks.iop.org/PPCF/47/269

Abstract

The poloidal distribution of turbulence in the scrape-off layer (SOL) of the CASTOR tokamak is studied by means of a ring of 32 electric probes covering the whole perimeter of the poloidal cross section. Analysis of floating potential fluctuations in a SOL created in the top part of the machine by shifting the plasma downwards reveals a dominant periodic structure that propagates poloidally in the direction of the $E_r \times B$ drift. Its poloidal mode number is found to be equal to the local safety factor q. Correlation and pulse propagation analyses show that this high m mode is a signature of a single long flute-like structure that is aligned with the magnetic field and snakes around the torus several times before terminating on the limiter.

(Some figures in this article are in colour only in the electronic version)

1. Introduction

Understanding the turbulence in the scrape-off layer (SOL) of tokamaks is as important as it is in the confined region. In most experimental conditions, the SOL transport is larger along the magnetic field lines except at the highest densities, as was shown in experiments in Alcator-CMod [1, 2]. However, cross-field transport still plays a significant role, because it defines the radial extent over which the power and the particles are deposited on limiters, divertors and other wall components in the SOL. The thickness of the power deposition layer is one of the most important problems [3, 4] facing the design of first wall components of the next

step machines, which cannot handle energy flux densities greater than $\sim$10 MW m^{-2}. This is particularly true with respect to edge localized modes (ELMs), which cause sudden bursts of energy flux, not only in the parallel direction but also in the perpendicular one [5]. In order to progress in the characterization of turbulent transport processes in the SOL, and eventually find ways to control them, special diagnostics with extremely high temporal and spatial resolution are needed.

Information about the spatial features of SOL turbulence in fusion machines has been mostly obtained by Langmuir probes (see, e.g. [6–8]), reflectometry (see, e.g. [9–11]), or beam emission spectroscopy [12, 13] but some recent results have been obtained with fast framing cameras in the visible domain [14, 15]. All experiments indicate the existence of coherent structures (lifetime greater than the mean auto correlation time) with typical lifetimes between 5 and 40 μs [16–19]. The poloidal correlation lengths are all of the order of 1 cm and the turbulence is found to propagate poloidally with a velocity compatible with the local $E_r \times B$ drift. Depending on the size of the machine, these coherent events may [20] or may not [6] survive a full poloidal turn. However, in most of these analyses, except in CCT [21, 22] where a poloidal array covering 60° was used, the radial and poloidal extents of the probe arrays are limited to a few correlation lengths so that, for example, the rotation of a structure around the poloidal section cannot be directly observed but must be deduced from poloidal velocity measurements.

In the experiment described here, we measure the poloidal structure of the turbulence using a poloidal ring of 32 electrodes uniformly distributed around the whole perimeter. This paper is organized as follows: in section 2, we describe the special probe diagnostics that were used in the experiment. The magnetic configuration of the SOL in the CASTOR tokamak, which is essential for the interpretation of experimental data is discussed in section 3. In section 4, the spatially resolved measurements of the SOL turbulence are presented. The results are discussed and conclusions are drawn in section 5.

2. Probe diagnostics used in the experiment

Measurements are performed in the CASTOR tokamak [23–25]. The major radius is $R = 0.4$ m. The small radius of the plasma is limited by the size of the poloidal ring which is $a = 5.8$ cm. The plasma current during the flat-top phase of the discharge can be varied in the range $I_p = 5$–10 kA. The line averaged density is $n_e = (0.5\text{–}1) \times 10^{19}$ m^{-3}. The toroidal magnetic field is $B_{tor} = 1.3$ T. The time evolution of the main parameters in a typical discharge is shown in figure 1.

The position of the plasma column is stabilized by the feedback system and, as seen from the corresponding traces in figure 1, it remains unchanged during the flat-top phase of a discharge. The edge safety factor $q(a)$ is calculated from the measurement of the total plasma current and toroidal magnetic field. The vertical shift of the plasma column, which results in a reduction of the plasma radius, is taken into account.

In the SOL region, the plasma density varies in the range $(0.2\text{–}0.5) \times 10^{19}$ m^{-3} and the electron temperature is 8–25 eV.

The poloidal ring (see figure 2) consists of 32 stainless steel plates of poloidal width 10 mm and toroidal length of 70 mm, each with a 2 mm diameter graphite Langmuir probe flush-mounted at its centre.

The ring of plates has a radius of 58 mm. Together with its supporting structure, it acts as a poloidal limiter and defines the toroidal angle 0°. All the plates are electrically insulated from each other as well as from the probes inserted in them. The signals are sampled at 1 MHz and synchronized. The layout of large plates with embedded probes is motivated by the fact that the

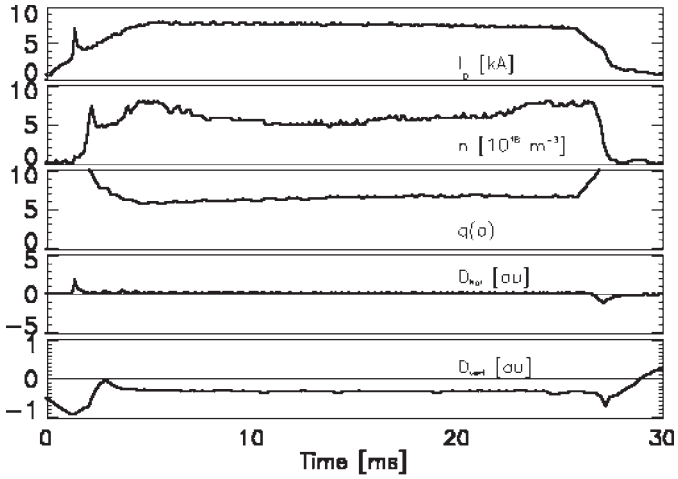

Figure 1. Time traces illustrating a typical scenario in CASTOR. From top to bottom: plasma current in kiloamperes (kA), line average density, calculated value of q at the last closed flux surface (LCFS) and the horizontal (D_{hor}) and vertical (D_{vert}) position of the plasma column (in arbitrary units).

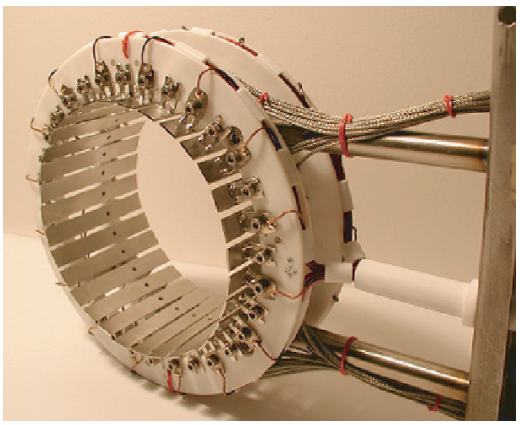

Figure 2. Photograph of the poloidal ring. It is composed of 32 stainless steel plates distributed uniformly around the poloidal perimeter at the radius $r = 58$ mm. Each plate is equipped with a flush-mounted Langmuir probe. All the plates and probes are electrically insulated from each other allowing independent measurement and biasing.

array was designed for experiments of active control of the electrostatic turbulence. However, in this paper only passive measurements are reported. All the plates and embedded probes are kept floating in these experiments. Whether the plates or the probes are used as sensors, no significant difference is found in the main turbulent features, despite the averaging effect due to the spatial extension of the plate. As a consequence, no distinction will be made hereafter. A numbering of the plates is adopted such that plate number 1 is located at the poloidal angle $\theta = 0^{\circ}$, that is, on the outboard midplane, and the numbering proceeds in the direction of increasing poloidal angles (towards the top, the inboard midplane and the bottom).

A rake probe, consisting of 16 tips facing the plasma, distributed radially with 2.5 mm spacing, is located at toroidal angle $\phi = 40^{\circ}$, on top of the torus corresponding to poloidal angle

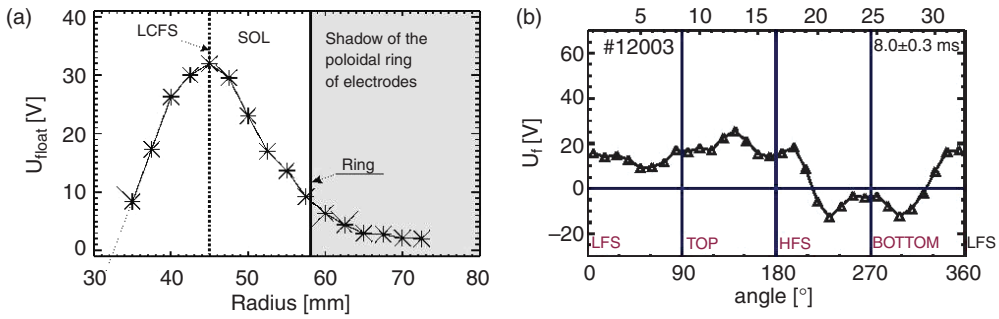

Figure 3. (*a*) Radial profile of the mean floating potential as measured at the top of the torus by the rake probe. The radial position of the top of the ring is marked by bars. (*b*) Distribution of the mean floating potential around the poloidal ring.

$\theta = 90^{\circ}$. The rake probe measures the radial profile of floating potential and its fluctuations. Its innermost tip is located at a vertical position of 50 mm relative to the centre of the vessel. A single Langmuir probe is located at $\phi = 180^{\circ}$, also on top of the torus. It is vertically positioned to be at the same radius as the poloidal ring. The correlation between signals measured by this probe and those measured by the poloidal ring, which are toroidally separated by 180°, can be calculated, giving complementary information about the orientation of the turbulent structures with respect to the magnetic field lines.

3. Magnetic configuration of the SOL

The magnetic configuration of the edge plasma on CASTOR, which is essential for correct interpretation of the fluctuation measurements, is deduced from the time-averaged floating potential measured by both probe arrays.

The typical radial profile of the time-averaged floating potential at the top of the torus as measured by the rake probe is shown in figure 3(*a*). It is seen that the maximum of the floating potential profile appears noticeably deeper than the leading edge of the poloidal ring. The radial position of the maximum marks the position of the velocity shear layer (see also [24, 25]), which is associated with the location of the last closed flux surface (LCFS).

The time-averaged floating potential measured around the poloidal ring is shown in figure 3(*b*). As seen from the figure, the top half of the ring (0–180°) measures a positive floating potential (10–15 V), which is consistent with the rake probe data measured at the same radius. This means that the top of the poloidal ring is immersed in the SOL plasma. The poloidal distribution of $V_{\rm float}$ is rather flat in this range of poloidal angles, which indicates that the probes at the top of the torus are located in the vicinity of the same magnetic surface.

On the other hand, the probes on the bottom part of the ring, in particular in the range of poloidal angles 210–330°, measure the negative floating potential, which is a signature that they are effectively well inside the confined region. This is also supported by measurements of the poloidal propagation velocity of fluctuations mainly determined by the $E_{\rm r} \times B_{\rm t}$ flow. The fluctuations at the bottom of the torus propagate poloidally in opposite directions at the bottom and at the top of the machine. This means that the top and bottom plates are on opposite sides of the shear layer, i.e. the bottom plates are in the confinement region.

All these measurements indicate that in the tokamak CASTOR, the magnetic flux surfaces are not concentric with the poloidal limiter. The respective position of the poloidal ring and

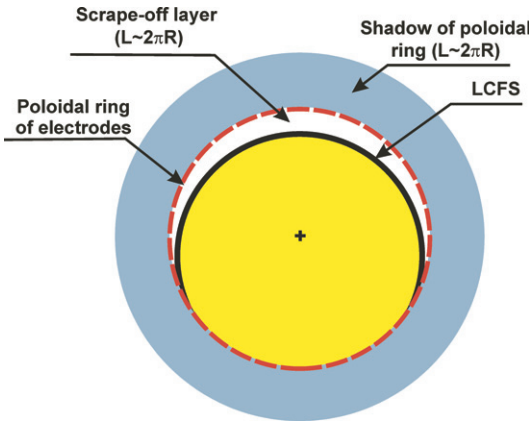

Figure 4. Respective position of the poloidal ring and the LCFS (schematic representation).

the last closed magnetic flux surface is schematically depicted in figure 4, which shows that the magnetic axis is shifted downward by several millimetres.

The SOL at the top of the torus consists of two regions with different parallel connection lengths. In the shadow of the poloidal limiter, the parallel connection length is limited to one toroidal turn, $L_{\parallel} \cong 2\pi R \cong 2.5$ m. The downshift of the plasma column creates a secondary SOL at the top of the machine having a crescent shape in the poloidal plane and a parallel connection length of several toroidal turns. As a consequence, the same field line intersects a given poloidal section several times, with the number of intersections being related to the local safety factor. Such a magnetic configuration with a long connection length in the SOL is equivalent to that in tokamaks equipped with a toroidal limiter or a divertor. It must be noted that, unfortunately, there are not enough magnetic loops available on CASTOR to reconstruct the shape of magnetic flux surfaces.

In order to prove additionally that the plates of the upper half of the ring are connected by magnetic field lines, a pulsed voltage is applied to a reference plate during the quasi-stationary phase of a discharge with edge safety factor $q(a) \sim 8$. The reference plate is located at the top of the poloidal ring at $\theta \sim 90^{\circ}$. The response to biasing is shown in figure 5, where an increase of the floating potential is observed on plates 32, 3, 11, 15 and 19, i.e. on every fourth plate starting from the reference plate.

The angular separation between these plates is consistent with the angle of the rotational transform ($\sim 22^{\circ}$) for this discharge. The floating potentials of the remaining plates are unchanged. This experimental observation is interpreted as a result of the formation of a single biased flux tube, which emanates from the biased reference plate and follows the helical magnetic field lines in both directions, upstream and downstream. The biased flux tube is detected simultaneously at different poloidal angles, since it extends more than five times around the torus in this particular case. Such a response is not observed on the bottom plates that are effectively located in the confinement region.

4. Spatially resolved measurements of fluctuations in the SOL

We first show in figure 6 the frequency spectrum of the floating potential fluctuations that is measured on one of the top plates of the poloidal ring. This spectrum shows that the potential fluctuations in CASTOR have a very broad frequency spectrum comparable to those usually observed in the SOL of other tokamaks.

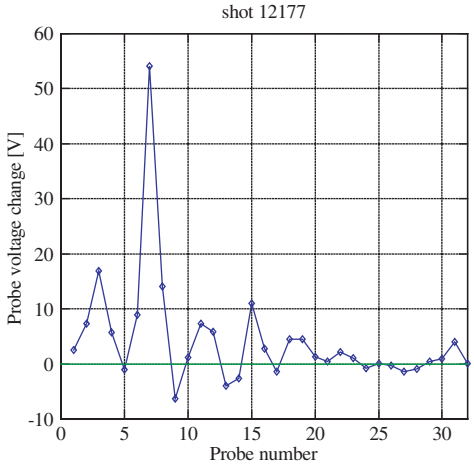

Figure 5. Response of the embedded probes of the poloidal ring to the voltage pulse (+180 V for 1 ms) applied to plate No. 7 located at $\theta \sim 90^{\circ}$ during the quasi-stationary phase of a discharge with edge safety factor $q(a) \sim 8$ (shot 12177). The picture shows the time averaged floating potential during the biasing phase. The average floating potential before the pulse application is subtracted.

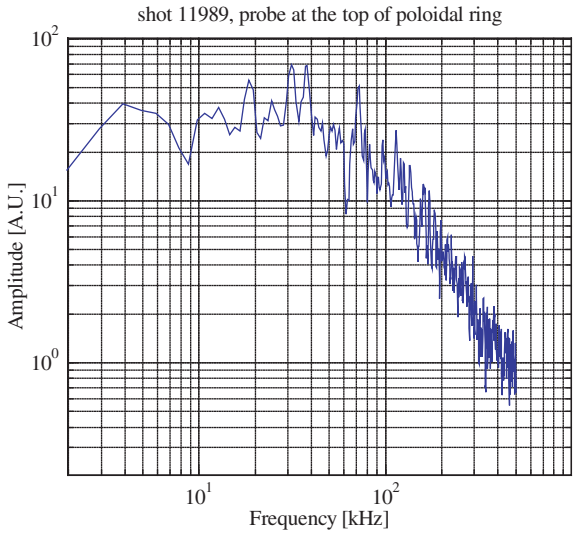

Figure 6. Frequency spectrum of floating potential fluctuations measured by the top probe of the poloidal ring ($\theta = 90^{\circ}$), shot 11989, $8 < t < 10$ ms.

The spatio-temporal diagram of the floating potential fluctuations measured by the top half of the poloidal array is shown in figure 7(*a*). The slow evolution, obtained by averaging over a moving window of 250 μs, has been subtracted from each signal, in order to focus on the fluctuations. Wave-like patterns propagating in the poloidal direction are clearly visible, exhibiting the presence of a dominant mode number ($m = 7$ in this case) and a period of 30 μs. The wave amplitude is not constant, but is modulated with a typical period of 100–150 μs. It is worth noting that the observed pattern has a similar amplitude on the low field side ($\theta = 0^{\circ}$) and on the high field side (around $\theta = 180^{\circ}$), so that the fluctuations do not show a ballooning

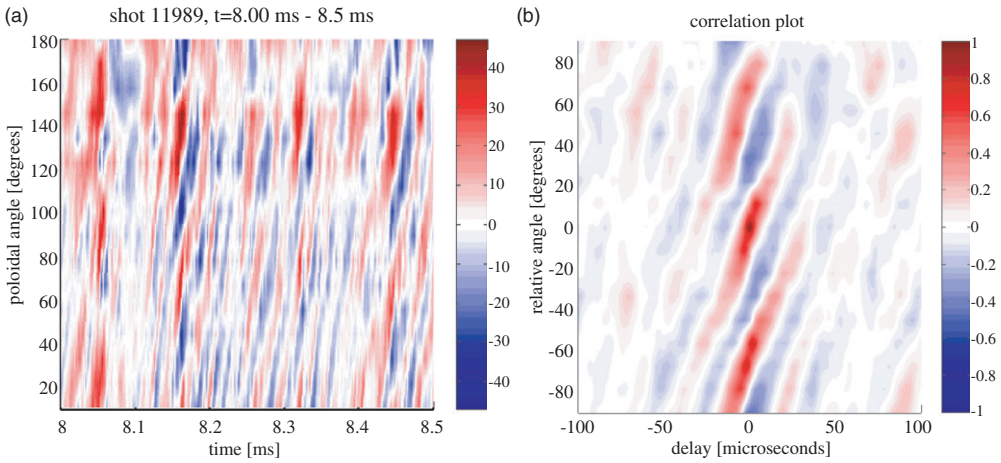

Figure 7. (*a*) Spatio-temporal plot of floating potential fluctuations measured by the poloidal array at the top half of the torus of the discharge. (*b*) Cross-correlation of the reference probe located at the top ($\theta \sim 90^{\circ}$) with the other probes of poloidal ring located in the top half of the torus.

character. In fact, the aspect ratio in CASTOR ($R/a = 7$) is not favourable for the occurrence of ballooning.

The correlation between a reference probe, which is located at the top of the torus, and all remaining probes of the top half of the ring is shown in figure 7(*b*). It can be seen that a significant correlation is found for times of the order of 100 μs. The presence of a dominant mode (with the poloidal mode number $m = 7$) is clearly seen from the regularity of the correlation pattern. The poloidal phase velocity of this mode is obtained from the inclination of the correlation pattern. At the top of the machine, the propagation direction is from the low to the high field side. This is consistent with the direction of the local $E_r \times B$ drift. The poloidal velocity is approximately $v_p \sim 3\,\mathrm{km\,s^{-1}}$ in this case and is comparable to that estimated from the measured radial electric field. The radial electric field is obtained from the gradient of the floating potential profile (see figure 3) neglecting the contribution of the electron temperature gradient. A more precise comparison would require the correction of the floating potential by the electron temperature but at this radial position, the electron temperature profile gradient is about $2\,\mathrm{eV\,cm^{-1}}$ with an uncertainty of $1\,\mathrm{eV\,cm^{-1}}$, a rather flat profile as is usually observed at these radii in CASTOR [25, 26] so that corrections due to temperature gradients would not be significant. For these shots, the upper plates of the poloidal ring are about $\Delta = 5$ mm away from the LCFS into the SOL because of the plasma downshift.

The temporal periodicity of signals measured by individual probes, which is clearly visible in figure 7, is a consequence of the poloidal rotation of the dominant poloidal Fourier mode. The characteristic frequency attributed to this effect is typically $f = mv_p/2\pi a \sim 20$–60 kHz in CASTOR. This effect has been discussed in [27], where the conditions for the observation of a time periodicity on the correlation pattern are given.

It must be noted that the density fluctuations cannot be measured in this configuration because the large surface of the plates and consequent unacceptable large magnitudes of the ion saturation current. However, the poloidally resolved information on density fluctuations is available in subsequent experiments [28] in which a poloidal ring with 124 small Langmuir probes evenly spaced has been used. The observed spatio-temporal structure of density fluctuations has been found to be very close to that of the floating potential shown above.

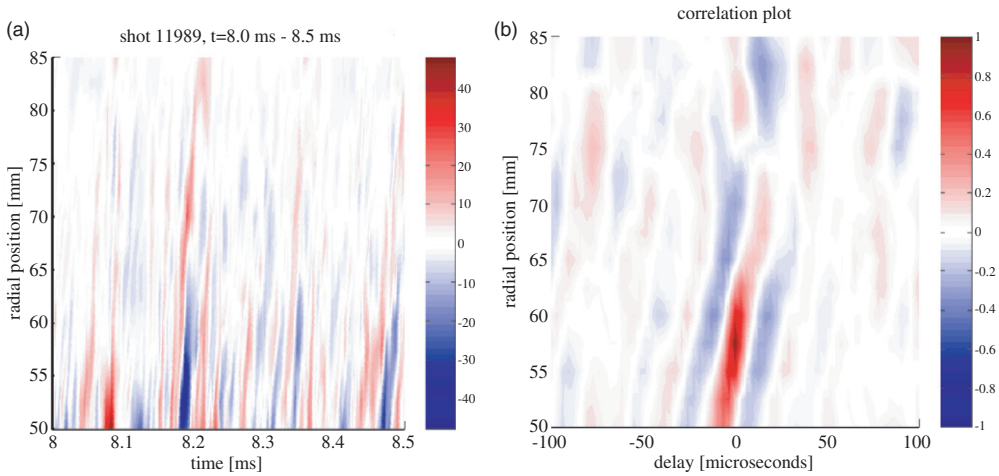

Figure 8. (*a*) spatio-temporal plot of the floating potential fluctuations measured by the rake probe at the top of the torus. Shot 11989, $8 < t < 8.5$ ms. (*b*) cross-correlation of rake probe tips with tip no. 3 of the same probe as a function of lag time. Shot 11989.

The rake probe measurements, shown in figure 8(*a*), indicate that the turbulent structures extend radially by at least 1 cm, and sometimes more. This is in agreement with previous measurements made with a two-dimensional array of probes [20]. The radial extent of the SOL turbulence is more precisely determined by the correlation analysis of the rake probe data, which is shown in figure 8(*b*). The tip used as the reference is the one located in the proximity of the same magnetic surface than the poloidal ring.

It is clearly seen from figure 8(*b*) that the radial correlation length of the potential fluctuations is indeed larger than $\sim$1 cm. The characteristic distance of the top plates from 'an average magnetic surface' is in the range of the vertical displacement of the plasma column, which is typically $\Delta \sim 5$ mm. Comparison of these two quantities shows that even if the plates of the ring lie on slightly different magnetic surfaces, they register the same turbulence features. Another interesting observation is the inclination of the patterns in the correlation plot shown in figure 8(*b*), which might be interpreted as a signature of a propagation of turbulence in the radial direction. However, the radial velocity deduced from the inclination angle (of the order of 600 m s^{-1}) is not the result of a radial plasma motion but is rather the result of the poloidal rotation of radially elongated structures, which are inclined along the poloidal direction. The reason for such inclination may be either the $E \times B$ flow gradient or the magnetic shear as discussed in [6, 7, 29].

Experiments in tokamaks and stellarators show that the turbulence remains correlated over a very long distance along a given magnetic field line [6, 7, 9]. The correlation can remain as high as 80% even for parallel lengths of the order of 10 m and also indicates that the parallel wave number $k_\parallel$ is much smaller than the perpendicular wave number $k_\perp$. In CASTOR the parallel correlation between the poloidal ring and a reference probe, located 180° toroidally away from the ring is studied. The reference probe is inserted in the SOL plasma from the top (the poloidal angle $\theta = 90°$) at the same radius as the poloidal ring. Figure 9 shows the correlation pattern between the reference probe and all the plates located at the upper half of the poloidal ring. The same poloidal periodicity of the correlation pattern is observed as in figure 7(*b*). This suggests that the turbulent structure associated with the reference probe crosses several times the poloidal ring.

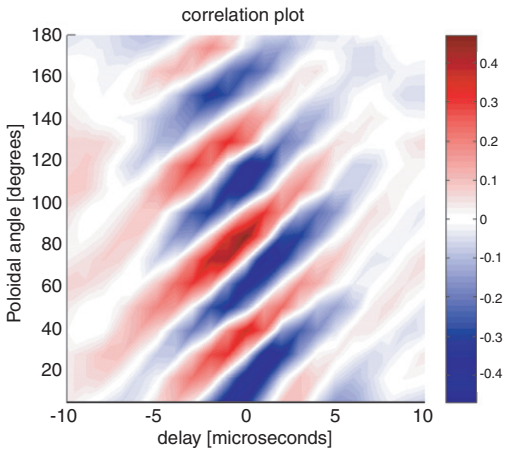

Figure 9. Cross-correlation pattern between the reference probe and plates of the poloidal ring at the upper half of the torus (0°–180°, shot 12009). The plate of the ring with the largest correlation level in the figure is poloidally separated by 17° and toroidally by 180° from the reference probe. All probes measure the floating potential.

The highest correlation magnitude is observed on the plate, which is poloidally and toroidally separated, respectively, by 17° and 180° from the reference probe. A calculation of the magnetic topology reveals that this two objects are directly magnetically connected for $q = 8$.

In order to check how the high-m mode adjusts to a change of magnetic helicity in the SOL, we have performed a scan of the edge safety factor by ramping down the plasma current. The poloidal mode number spectrum has been determined by applying a sliding spatial Fourier transform on the fluctuation data of the poloidal ring. The resulting temporal evolution of the poloidal mode number spectrum is shown in figure 10, where the evolution of the local safety factor q is also plotted. The broadness of the spectrum confirms that the $m = q$ mode is superposed on a broadband turbulent spectrum. It is clearly seen that the dominant poloidal mode number of the spectrum and the safety factor behave in the same way. This demonstrates again that the local B field helicity creates a dominant spatial Fourier mode in the poloidal spectrum of the SOL turbulence.

It can be noticed, however, that the m number measured by the poloidal ring seems to be less than the q value at the edge at the lowest plasma currents. This discrepancy is probably caused by a slight increase of the plasma radius during this phase of the discharge, which can lead to overestimation of the calculated $q(a)$ value.

An alternative explanation of the change of the dominant poloidal mode with the q value could be the existence of an $m/n = q/1$ MHD mode in the plasma. However, this possibility must be discarded because such a mode cannot exist in the SOL where the magnetic field lines are opened and so far the MHD activity with $m \sim q(a)$ has never been detected by Mirnov coils in CASTOR .

5. Discussion and conclusions

The probe measurements have allowed to demonstrate that, in the situation with downward shifted plasma, the SOL of CASTOR is composed of two regions with different parallel connection lengths. The region close to the wall is in the shadow of the poloidal ring and has a

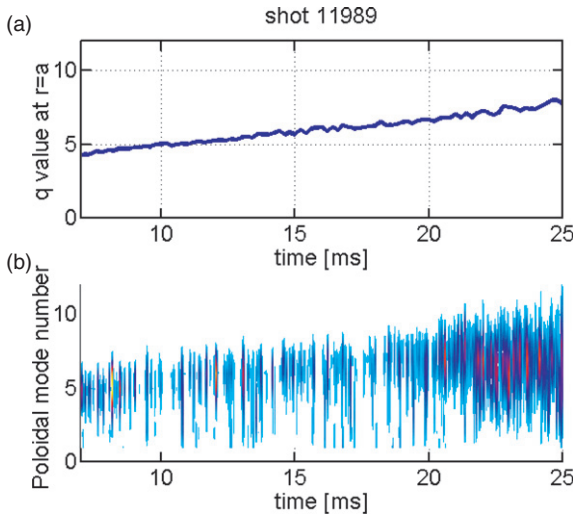

Figure 10. (*a*) change of the edge safety factor q during *a* discharge with plasma current ramp down. (*b*) temporal evolution of the poloidal mode number spectrum in the SOL during the same discharge.

parallel connection length equal to one toroidal turn. A secondary SOL, created because of the plasma downshift, is observed in the upper half of the chamber. In this region the B field lines snake several times around the torus and finally terminate on the poloidal limiter. In fact, this region is similar to divertor or toroidal limiter SOL configuration. Its length is determined by the local safety factor q and by the vertical displacement Δ of the plasma column. The pulse propagation experiment reveals that the parallel connection length in the secondary SOL is at least $\sim 5 \times 2\pi R$ for the typical safety factor $q \sim 8$.

The correlation analysis of potential fluctuations, performed using as a reference either one plate of the poloidal ring or a probe located at another toroidal angle, indicates that the behaviour of the SOL turbulence is strongly linked to the configuration of the magnetic field in this region. The fluctuation measurements could be interpreted in a straightforward way assuming a single long structure aligned with the magnetic field lines, which intersects a given poloidal cross section several times, giving rise to an apparent $m = q$ mode. This structure propagates in the poloidal direction at a velocity of the order of the local $E_r \times B$ drift. The alternating sign of the correlation pattern observed in figure 7(*b*) indicates a dipole character of the structure, which is also observed in other machines [16, 29, 30].

A possible explanation comes from the flute-like instability model in the SOL described in [31, 32]. The model is based on the curvature and gradient of the magnetic field and predicts fluctuating parallel currents flowing in the SOL to the surface of the limiter. These currents charge flux tubes connected to the limiter at different potentials. In order to obtain the observed periodicity, it is necessary that only a single turbulent feature having a dipole poloidal structure exists. In that case, the helicity of the field line would reproduce the same dipole feature at different poloidal positions and would give a correlation pattern on the ring similar to the one shown in figure 7. The model of Nedospasov [31] has been adopted by Endler *et al* [6] to describe the SOL turbulence in the tokamak ASDEX where individual fluctuation events with a dipolar structure and propagating poloidally have been observed. However, the typical wavelength measured in ASDEX was much lower than would be expected from the simple $m = q(a)$ condition.

Indeed, the model of Nedospasov [31] requires a material surface with respect to which different magnetic flux tubes can be charged to different potentials. Hence, the configuration and size of the limiter/divertor will determine the number of flute like structures that can be excited simultaneously. In the case of CASTOR with a small poloidal limiter, only one such structure can fit into the available volume whereas several of them can be excited simultaneously in ASDEX, giving rise to a correlation pattern with several poloidal oscillations.

Acknowledgments

Authors are indebted to F Jiranek, V Havlik, K Rieger, M Satava and J Zelenka for the design, construction of diagnostics and technical assistance in the experiment. This work has been carried out with the support of the projects No 202/03/0786 (Grant Agency of the Czech Republic) and No 2001-2056 (INTAS).

References

[1] Umansky M V, Krasheninnikov S I, LaBombard B and Terry J L 1998 *Phys. Plasmas* **5** 3373
[2] LaBombard B, Umansky M V, Boivin R L, Goetz J A, Hughes J, Lipschultz B, Mossessian D, Pitcher C S, Terry J L and Alcator Group 2000 *Nucl. Fusion* **40** 2041–60
[3] Federici G *et al* 2003 *J. Nucl. Mater.* **313–316** 11
[4] Stangeby P C and McCracken G M 1990 *Nucl. Fusion* **30** 1225
[5] Fundamenski W, Sailer W and JET EFDA contributors 2004 *Plasma Phys. Control. Fusion* **46** 233
[6] Endler M, Niedermeyer H, Giannone L, Holzauer E, Rudyj A, Theimer G, Tsois N and the ASDEX Team 1995 *Nucl. Fusion* **35** 1307
[7] Bleuel J, Endler M, Niedermeyer H, Schubert M, Thomsen H and the W7-AS Team 2002 *New J. Phys.* **4** 38
[8] Petržílka J and Stöckel J 1998 Edge turbulence analysis by means of electrical probes on tokamak CASTOR *Contrib. Plasma Phys.* **38** 74–9
[9] Vershkov V A, Soldatov S V, Shelukhin D A and Chistiakov V V 1999 *Nucl. Fusion* **39** 1783
[10] Bruskin L G, Mase A, Oyama N, Shinohara K and Miura Y 2003 *Plasma Phys. Control. Fusion* **45** 1227–45
[11] Ribeiro T T, Serra F, Conway G D, Manso M E, Ryter F, Cupido L, Kurzan B, Silva A, Suttrop W, Vergamota S and ASDEX Upgrade Team 2001 *Rev. Sci. Instrum.* **72** 1366–71
[12] McKee G R, Ashley R, Durst R, Fonck R, Jakubowski M, Tritz K, Burrell K, Greenfield C and Robinson J 1999 *Rev. Sci. Instrum.* **70** 913
[13] McKee G R, Fenzi C, Fonck R J and Jakubowski M 2003 *Rev. Sci. Instrum.* **74** 2014–19
[14] Zweben S J *et al* 2002 *Phys. Plasmas* **9** 1981
[15] Terry J L *et al* 2003 *Phys. Plasmas* **10** 1739–47
[16] Joseph B K, Jha R, Kaw P, Mattoo S K, Rao C V S, Saxena Y C and the ADITYA Team 1997 *Phys. Plasmas* **4** 4292
[17] Carreras B A, Hidalgo C, Sanchez E, Pedrosa M A, Balbin R, Cortes I G, Van Milligen B, Newman D E and Lynch V E 1995 *Phys. Plasmas* **2** 839
[18] Pericoli-Ridolfini V, Pietropaola A, Cesario R and Zonca F 1998 *Nucl. Fusion* **38** 12
[19] Moyer R A, Lehmer R D, Evans T E, Conn R W and Schmitz L 1996 *Plasma Phys. Control. Fusion* **38** 1273
[20] Martines E, Hron M and Stöckel J 2002 *Plasma Phys. Control. Fusion* **44** 351
[21] Tynan G R, Schmitz L, Conn R W, Doerner R and Lehmer R 1992 *Phys. Rev. Lett.* **68** 3032
[22] Tynan G R, Liberati J, Pribyl P, Taylor R J and Wells B 1996 *Plasma Phys. Control. Fusion* **38** 1301–5
[23] Stockel J *et al* 1999 *Plasma Phys. Control. Fusion* **41** A577–A585
[24] Van Oost G, Stöckel J, Hron M, Devynck P, Dyabilin K, Gunn J, Horacek J, Martines E and Tendler M 2001 *11th Int. Toki Conf. on Potential and Structure in Plasmas (Toki, Japan, 5/12/00–8/12/00) J. Plasma Fusion Res.* Series **4** 29
[25] Van Oost G *et al* 2003 *Plasma Phys. Control. Fusion* **45** 621
[26] Gunn J *et al* 2001 *Czech. J. Phys.* **51** 1001

[27] Devynck P, Stockel J, Adamek J, Duran I, Hron M and Van Oost G 2003 *Czech. J. Phys.* **53** 853
[28] Sstockel J *et al* 2003 *Proc. 30th EPS Conf. on Controlled Fusion and Plasma Physics (St Petersburg, July 2003)* vol 27A (ECA) P-1.179
[29] Bruchhausen M, Burhenn R, Endler M, Kocsis G, Pospieszczyk A, Zoletnik S and the W7-AS Team 2004 *Plasma Phys. Control. Fusion* **46** 489–505
[30] Spolaore M, Antoni V, Bergsaker H, Cavazzana R, Drake J, Martines E, Regnoli G, Serianni G, Spada E and Vianello N 2003 *Proc. 30th EPS Conf. on Controlled Fusion and Plasma Physics (St Petersburg, Russia, July 7–11)* pp 2–158
[31] Nedospasov A V 1989 *Sov. J. Plasma Phys.* **15** 659
[32] Garbet X, Laurent L, Roubin J P and Samain A 1991 *Nucl. Fusion* **31** 967